npj | climate and atmospheric science

Article

Published in partnership with CECCR at King Abdulaziz University

https://doi.org/10.1038/s41612-025-00913-4

Multifaceted changes in water availability with a warmer climate

Binglan Gu[1,2], Sha Zhou[1,2] ✉, Bofu Yu[3], Kirsten L. Findell[4] & Benjamin R. Lintner[5]

Climate warming alters spatial and seasonal patterns of surface water availability (P-E), affecting runoff and terrestrial water storage. However, a comprehensive assessment of these changes across various hydroclimates remains lacking. We develop a multi-model ensemble approach to classify global terrestrial hydroclimate into four distinct regimes based on the mean and seasonality of P-E. P-E is projected to become increasingly variable across space and time. Wet regions with low and high seasonality are likely to experience more concentrated increases in wet-season runoff by up to 20%, highlighting potential increases in flood-related vulnerability. Low-seasonality regions exhibit faster wet-season increases and more rapid dry-season decreases in soil moisture, heightening the likelihood of water scarcity and drought. Conversely, dry regions with high seasonality are less sensitive to climate change. These findings underscore the multifaceted impacts of climate change on global water resources, necessitating the need for tailored adaptation strategies for different hydroclimate regimes.

Surface water availability is the difference between water supply from precipitation and water loss through evaporation and determines the spatial and temporal variations in runoff and terrestrial water storage over land[1–3]. Changes in water availability have widespread implications for human well-being, socioeconomic development, and ecosystem sustainability[4,5]. Global warming is expected to enhance the spatial and temporal variability in water availability, broadly leading to a "wet get wetter, dry get drier" (WWDD) scenario in both space and time[6–10]. Circulation changes and land-atmosphere feedback may cause deviations from the WWDD pattern over many regions[11–14]. While previous studies have extensively examined changes in the annual mean and seasonal variability of precipitation, evaporation, and water availability separately[3,15–20], a joint analysis of climate change impacts on the spatial and seasonal patterns of wetting and drying trends is lacking. Moreover, it remains unknown whether these changes would preferentially affect runoff or terrestrial water storage over different regions and seasons, which are vital for societal and ecological vulnerability to changes in water availability.

Societies and ecosystems are sensitive to the annual mean and particularly the seasonality of water availability[5,21]. Amplification of surface water seasonality in a warming climate may alter or disrupt water supply for human and ecological needs, and may even lead to more frequent and/or intense droughts and floods, posing great challenges to the sustainable management of water resources[22–24]. In addition to changes in water availability, e.g. the mean, seasonality, and extremes, the societal and ecological impacts also depend on regional hydroclimate characteristics[15] and how changes in water availability are partitioned into changes in runoff and terrestrial water storage gain/loss[2,25]. When increases in water availability are partitioned more heavily towards surface runoff in the wet region/season, this would increase the frequency and severity of floods, while terrestrial water storage gain may moderate the flood risk[26,27]. On the other hand, decreases in water availability, particularly in the dry region/season, may induce hydrological drought (low runoff) and/or agricultural drought (low soil moisture), as well as flash drought due to rapid decreases in soil moisture[28–30]. It is therefore important to consider and assess the joint changes in the mean and seasonality of water availability and how these changes affect runoff and terrestrial water storage gain/loss over different regions and seasons.

In this study, we develop a multi-model ensemble approach to identify four distinct hydroclimate regimes combining climatological mean and seasonal variability and use a comprehensive framework to examine future shifts in the mean and seasonal cycle of water availability and associated changes in runoff and terrestrial water storage over different regimes. We assess the spatial and seasonal patterns of hydroclimate changes between the historical (1971–2000) and future (2071–2100) periods, using 17 global climate models from the Coupled Model Intercomparison Project phase 6 (CMIP6)[31] (Table S1). For future projections, two extreme emission scenarios, i.e. ssp1-2.6 and ssp5-8.5, were used to evaluate the range of change in several critical hydroclimate variables, namely, precipitation (P), evaporation (E), surface water availability (P-E), runoff (R), and terrestrial water

[1]State Key Laboratory of Earth Surface Processes and Resource Ecology, Faculty of Geographical Science, Beijing Normal University, Beijing, China. [2]Institute of Land Surface System and Sustainable Development, Faculty of Geographical Science, Beijing Normal University, Beijing, China. [3]School of Engineering and Built Environment, Griffith University, Nathan, QLD, Australia. [4]NOAA/Geophysical Fluid Dynamics Laboratory, Princeton, NJ, USA. [5]Department of Environmental Sciences, Rutgers, The State University of New Jersey, New Brunswick, NJ, USA. ✉e-mail: shazhou21@bnu.edu.cn

storage gain/loss with time (d*S*/d*t*) for the four hydroclimate regimes. These multifaceted analyses enable a comprehensive understanding of climate change impacts on terrestrial water cycle and water resources, elucidating the hydrological implications for both society and ecosystems.

Results

Global distribution of hydroclimate regimes

Global terrestrial hydroclimate is classified into four distinct regimes based on the median thresholds of climatological mean P-E and precipitation seasonality, the latter is quantified as the relative entropy (RE) of monthly precipitation (see "Methods" and Fig. 1). RE has been widely used as a non-parametric seasonality metric for precipitation[19,32] and is useful for identifying dry season length[33]. As the seasonal cycle of P-E is largely driven by that of precipitation and the seasonal variations of P and P-E are consistent across most land areas (Figs. 1c–f and S1), the RE of precipitation is used to measure the hydroclimate seasonality. Higher RE values indicate higher seasonality, and vice versa.

The spatial distribution of the four regimes (HH, HL, LH, and LL; see Fig. 1 caption for regime definitions) based on the 17 climate models, as well as the aggregated seasonal cycles of P, E, and P-E for each regime, are shown in Fig. 1. Both the spatial pattern of hydroclimate regimes and the seasonal cycles of hydroclimate variables are consistent with those from the ERA5 reanalysis[34] and observation-based datasets of GPCC precipitation[35] and GLEAM evaporation[36] (Figs. 1 and S1). This consistency indicates that the multi-model ensemble effectively represents the historical hydroclimate characteristics. Additionally, the multi-model ensemble effectively captures hydroclimate characteristics across different models and between historical and future periods (Figs. S2 and S3).

The regime HH exhibits high P-E and high precipitation seasonality and is mostly found in tropical and temperate monsoon regions, covering 24.8% of land areas (Fig. 1a–c). Affected by the monsoon climate, both P and P-E are concentrated in wet months, but P-E turns negative in dry months, when evaporation from moist soils increases due to high atmospheric evaporative demand[9] (Fig. 1c). These regions face challenges in managing water resources to mitigate seasonal floods and droughts, and they may also be vulnerable to future climate change impacts[23,37]. In contrast, the regime HL has high P-E but low precipitation seasonality, indicating more reliable water availability throughout the year (Fig. 1b, d). Occupying 23.2% of land areas, the HL regime is found across almost all latitudes, including the equatorial zone (largely co-located with humid tropical rainforests), Europe, and eastern and northwestern parts of North America (Fig. 1a). Collectively, regions with HH and HL occupy global humid regions and are denoted as

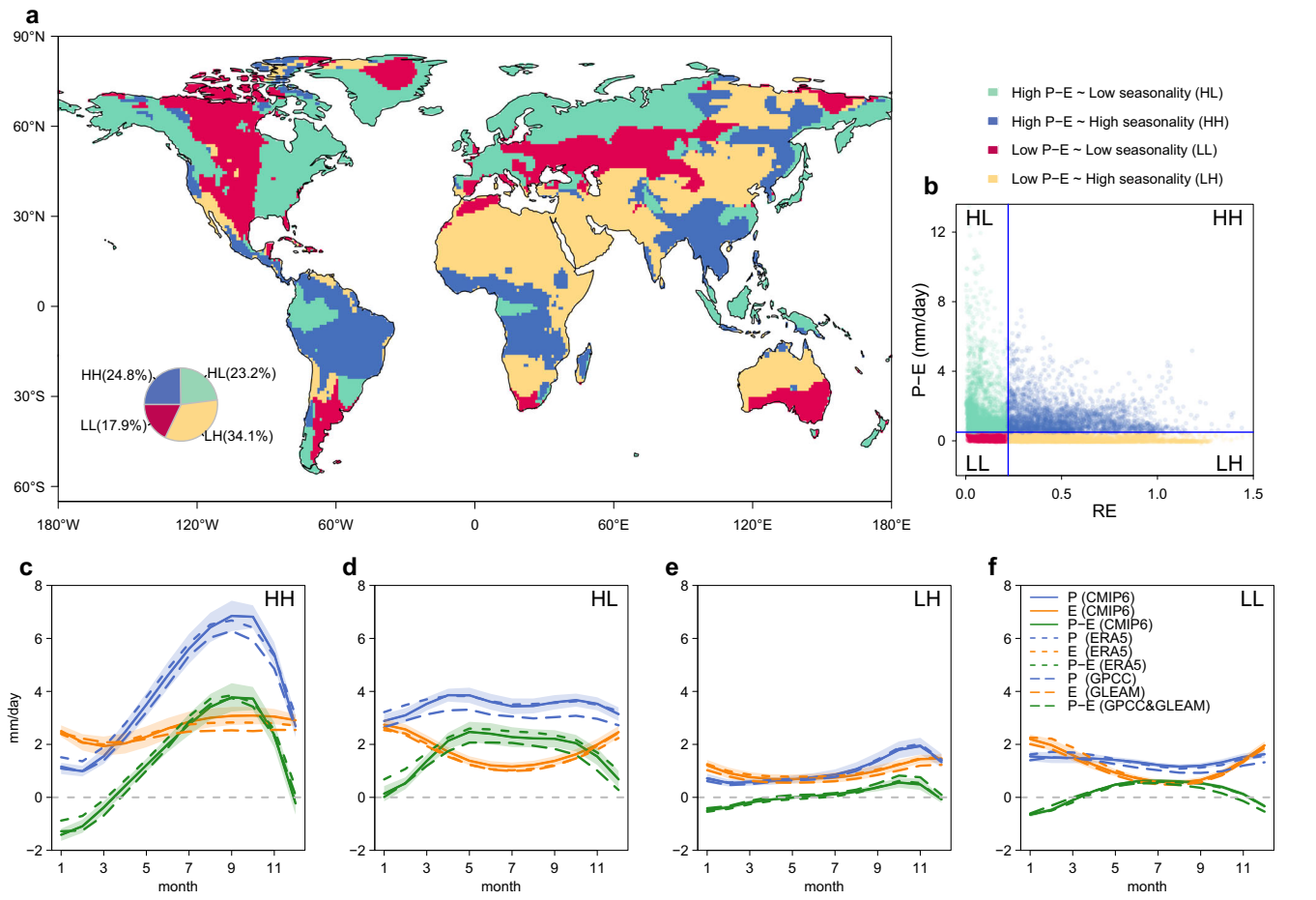

Fig. 1 | Global distribution of hydroclimate regimes. a The global distribution of four hydroclimate regimes based on the median (i.e., 50th percentile) thresholds of the multi-model mean water availability (P-E) and relative entropy (RE) of precipitation as a measure of hydroclimate seasonality (see "Methods"). P-E and RE are calculated using the historical simulations (1971–2000) of 17 climate models in CMIP6. The pie plot insets shows the proportion of land areas for the four regimes. The first letter represents the high (H) or low (L) level of the mean P-E and the second letter for the level of hydroclimate seasonality. **b** Distribution of the multi-model mean P-E and RE across land grid cells, and the median thresholds are shown as blue lines. **c**–**f** Monthly mean precipitation (*P*), evaporation (*E*), and surface water availability (P-E) in the regime HH (**c**), HL (**d**), LH (**e**), and LL (**f**) based on multi-model means (solid lines), the ERA5 reanalysis (dashed lines), and the combination of GPCC precipitation and GLEAM evaporation (long dashed lines) in the historical period (1971–2000). The shading shows one standard deviation of the hydroclimate variables across the 17 climate models. The order of 12 months in the *x*-axis starts from the month with the lowest mean P-E during the historical period for each grid cell and the mean seasonal cycle across all grid cells of each regime is shown in (**c**–**f**).

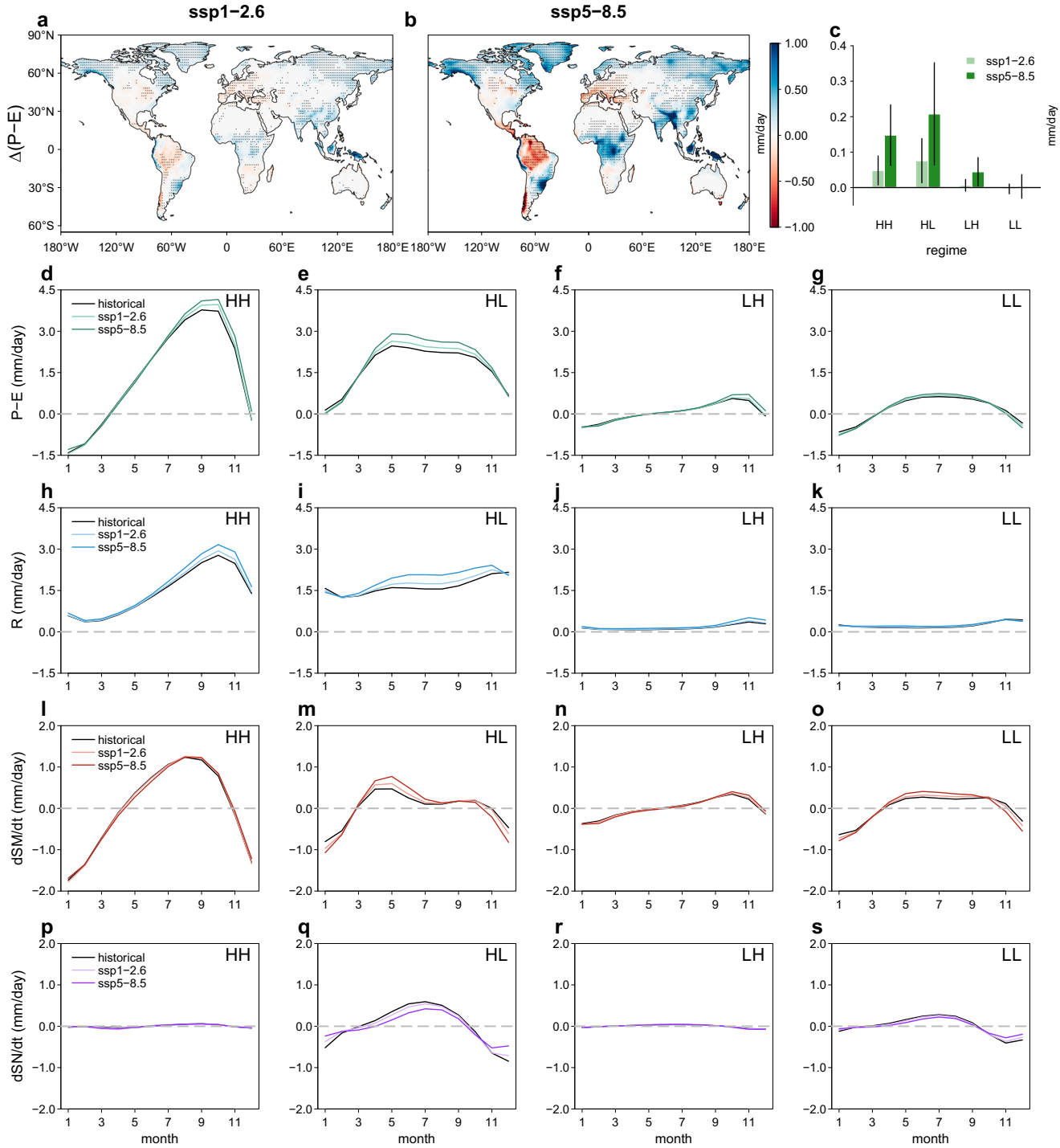

Fig. 2 | Multi-model mean changes in water availability between the historical and future periods. a, **b** Changes in water availability (Δ(P-E)) between the historical (1971–2000) and future (2071–2100) periods under the ssp1-2.6 (**a**) and ssp5-8.5 (**b**) scenarios. The dotted areas denote the sign of Δ(P-E) is consistent with the sign of multi-model means for more than 75% (at least 13) of the 17 models, which ensures that the change in P-E is significant (p-value < 0.05) based on multi-model agreement. **c** The same as (**a**, **b**), but for the area-weighted mean Δ(P-E) for the four regimes HH, HL, LH, and LL shown in Fig. 1. The error bars show the standard deviation of Δ(P-E) across the 17 models. **d**–**g** Mean seasonal cycles of P-E for the four regimes during the historical and future (ssp1-2.6 and ssp5-8.5) periods. **h**–**s** The same as (**d**–**g**), but for runoff (R, **h**–**k**), changes in soil moisture (dSM/dt, **l**–**o**) and snow amount (dSN/dt, **p**–**s**) over time. Month 1 along the x-axis is associated with the month with the lowest P-E during the historical period.

wet regimes. The dry regimes LH and LL are mostly located in subtropical dryland areas with both low P and P-E, and each of them covers 34.1% and 17.9% of land areas, respectively (Fig. 1a, e, and f). Due to water scarcity experienced in both wet and dry seasons, these regions are inherently arid and face elevated risks of droughts, particularly in a warming and drying climate[38].

Spatial and temporal patterns of changes in water availability

Based on the agreement of 17 CMIP6 models, we find significant changes in P-E over 41% of the land area with the low emission scenario and 58% with the high emission scenario, similar to a previous study[39] (Fig. 2a, b). The spatial pattern of P-E changes between the two scenarios is highly consistent, with the spatial correlation coefficient (r) of 0.90, and the magnitude of P-E

changes, both increases and decreases, is more pronounced for the higher emission scenario. Increases in P-E are found mostly in the two wet regimes with high P-E (HH and HL), while decreases occur mainly in the dry regimes (LL and LH) (Fig. 2a–c), suggesting an amplified spatial pattern of P-E in future projections.

Seasonal variations in P-E and their future shifts affect both runoff and terrestrial water storage (including soil moisture and snow amount) over different regions. The seasonal cycles of P-E, runoff, monthly changes in soil moisture (d*SM*/d*t*) and snow amount (d*SN*/d*t*) over time are aggregated over the four hydroclimate regimes during the historical (1971–2000) and future (2071–2100, ssp1-2.6 and ssp5-8.5) periods (Figs. 2d–s and S4a–p). For the HH regime, future hydroclimate seasonality is enhanced with projected increases in the peak P-E and runoff, while seasonal cycles of d*SM*/d*t* and d*SN*/d*t* are similar between historical and future periods (Fig. 2d, h, l, and p). For most HH areas with increased P-E, both P-E and runoff are projected to be even more concentrated in wet months (Fig. S5a, e). This could lead to a surplus in water supply, posing challenges for water resources management, particularly under the high-emission scenario. In contrast, for some HH areas where reductions in P-E are projected, such as the Amazon, the peak and seasonality of P-E and runoff are projected to decrease (Fig. S5b, f), indicating a strong drying trend during wet months.

Across the four regimes, the HL regime experiences the greatest increase in mean P-E in future projections (Fig. 2c). While the increase in P-E in HL is more evenly distributed compared to HH, the seasonality of P-E is enhanced regardless of whether climatological mean P-E increases or decreases (Figs. 2e and S5c, d). However, the seasonal responses of runoff, d*SM*/d*t*, and d*SN*/d*t* to this enhanced P-E seasonality vary across different regions (Figs. 2i, m, and q and S6). In snow-free regions, the seasonality of runoff is amplified, while the seasonal cycle of d*SM*/d*t* remains largely unchanged (Fig. S6b, f, and j). Conversely, in snow-covered regions, runoff seasonality is reduced, and the seasonal cycles of d*SM*/d*t* and d*SN*/d*t* are projected to shift in an opposite manner (Fig. S6e, i, and m). In dry months (d*SM*/d*t* < 0), we find faster declines in SM, likely because of reduced P-E arising from higher evaporative demand of a warmer atmosphere and less snowmelt to recharge SM; similarly, SM increases more rapidly due to increased P-E and delayed snow accumulation in wet months (Fig. S6a, i, and m). As precipitation tends to fall as rain instead of snow in a warming world[40,41], the rate and magnitude of snow accumulation decrease in the cold and wet months, resulting in reduced snowmelt water supply as runoff and SM to meet water demand in the warm and dry months[42,43].

Compared to the wet regimes, changes in mean P-E are less evident in the two dry regimes LH and LL, while the seasonality of P-E is also enhanced in the high-emission scenario (Fig. 2c, f, and g). Similar to the HH regime, seasonal change in P-E, i.e. increased P-E in wet months, primarily affects runoff for LH, with minor alterations in the seasonal cycles of d*SM*/d*t* and d*SN*/d*t* (Fig. 2f, j, n, and r). Increasing P-E and runoff occur mainly in East Africa and North Asia, which alleviate water scarcity in these arid regions (Fig. 2a, b and see Fig. 1a for LH). In contrast, little change in runoff throughout the year is evident for the regime LL (Figs. 2k and S6g, h). Future seasonal changes in P-E enhance the seasonality of d*SM*/d*t*, while the seasonality of d*SN*/d*t* is reduced in snow-covered regions (Fig. 2g, o, and s and Fig. S6c, k, and o). The opposing seasonal shifts in d*SM*/d*t* and d*SN*/d*t* are similar to those for HL, resulting in less snowmelt and more rapid declines in SM that aggravate water scarcity in dry months.

Future changes in water availability in wet and dry seasons

To further illustrate the seasonal changes in P-E over land and how they affect runoff and terrestrial water storage, we examine future changes of these hydroclimate variables under ssp5-8.5 (2071–2100) during the wet and dry seasons, which are defined as three consecutive months with the highest and lowest mean P-E in the historical period (1971–2000)[13]. In addition to the enhanced spatial pattern of P-E, the seasonal pattern of P-E is also significantly intensified over 49% of land areas, which provides evidence for the paradigm of WWDD in seasonality over about half of global land areas[9] (Fig. 3a–c). In contrast, the seasonality of P-E is reduced, i.e. showing an opposing pattern of WDDW, over the Amazon and many sub-tropical regions (Fig. 3a–c), where SM is projected to decrease[33,38] (Fig. S7). This enhanced SM limitation reduces evaporation while simultaneously enhancing moisture convergence through SM-atmosphere feedback, resulting in smaller reductions in precipitation compared to evaporation and hence increased P-E in the dry season[12,13]. As this negative SM feedback on P-E is rather weak in the wet season, P-E decreases as a result of climate change[12,13]. These processes lead to a diminished hydroclimate seasonality in future projections.

Seasonal changes in runoff closely resemble those of P-E, with the annual range of runoff being amplified over many humid regions but diminished in the Amazon (Fig. 3d–f). Additionally, we find widespread changes in the rate of terrestrial water storage gain/loss (Fig. 3g, h). Elevated P-E accelerates the rate of water storage accumulation in the wet season, while reduced P-E expedites water storage depletion in the dry season (Fig. 3a, b, g, and h). As global warming reduces the probability of snowfall and advances the timing of snowmelt[40], the rates of snow accumulation and snowmelt (d*SN*/d*t*) are projected to slow down during wet and dry seasons in high-latitude snow-covered regions (Fig. 3k, l). This undermines the snowpack's capacity to retain cold and wet season precipitation and thereby limits its ability to replenish runoff and SM in the warm and dry seasons[44,45]. Owing to the joint effect of seasonal changes in P-E and d*SN*/d*t*, seasonal differences in d*SM*/d*t* are greatly amplified, resulting in more pronounced increases and decreases of SM in the wet and dry seasons, respectively (Fig. 3i, j). Conversely, the diminished seasonality of P-E in the Amazon and sub-tropical dry regions weakens the seasonal variations in SM, resulting in reduced wet-season d*SM*/d*t* and increased dry-season d*SM*/d*t* (Fig. 3i,j). These seasonal changes in hydrological terms persist even in the low emission scenario (ssp1-2.6), albeit to a lesser extent, suggesting the significant and inevitable alterations in the terrestrial water cycle under climate change (Fig. S8).

Aggregated over the four regimes, increases in wet-season P-E primarily drive runoff to increase, particularly for the wet regimes, where runoff increases by 0.15–0.39 mm/d (8–20%) for HH and 0.19–0.49 mm/d (7–17%) for HL, based on the multi-model ensemble under scenarios ssp1-2.6 to ssp5-8.5 (Figs. 3m and S8m). Notably, wet-season runoff can increase by as much as 0.94 mm/d for HH and 0.86 mm/d for HL for some models. In contrast, changes in runoff during the dry season are relatively small for the four regimes (Figs. 3n and S8n). Additionally, seasonal contrasts in d*SM*/d*t* are strengthened, while contrasts in d*SN*/d*t* are diminished, for the low seasonality regimes HL and LL, driven by climate warming and enhanced annual range of P-E (Fig. 3m, n). The rate of increase in wet-season SM is amplified by 0.14–0.32 mm/d for HL and by 0.08–0.19 mm/d for LL (Figs. 3m and S8m). Conversely, the rate of SM decline during the dry season is intensified by 0.12–0.23 mm/d for HL and by 0.07–0.14 mm/d for LL (Figs. 3n and S8n). These findings highlight the considerable hydrological repercussions of climate change, potentially leading to heightened flood risks in the wet regimes and increased likelihood of water scarcity and droughts in the low seasonality regimes, especially for LL, which is already arid during the historical period.

Compounding effects of precipitation and evaporation on water availability

Given that water availability hinges on the balance of precipitation and evaporation, we further assess their future changes and their compounding effects on water availability, runoff and terrestrial water storage. The spatial patterns of changes in the mean precipitation and evaporation are highly correlated (spatial $r = 0.71$ in ssp1-2.6 and $r = 0.66$ in ssp5-8.5, Fig. 4a, b, d, and e). This suggests that projected changes in precipitation are primarily offset by corresponding adjustments in evaporation, and the interplay between precipitation-driven water gain and evaporation-induced water loss leads to altered P-E over the four regimes (Fig. 4c, f). For the dry regimes (LH and LL), increases in precipitation are largely offset by those of evaporation, resulting in small changes in P-E (Figs. 2c and 4c, f). As evaporation is primarily constrained by available energy in the wet regimes

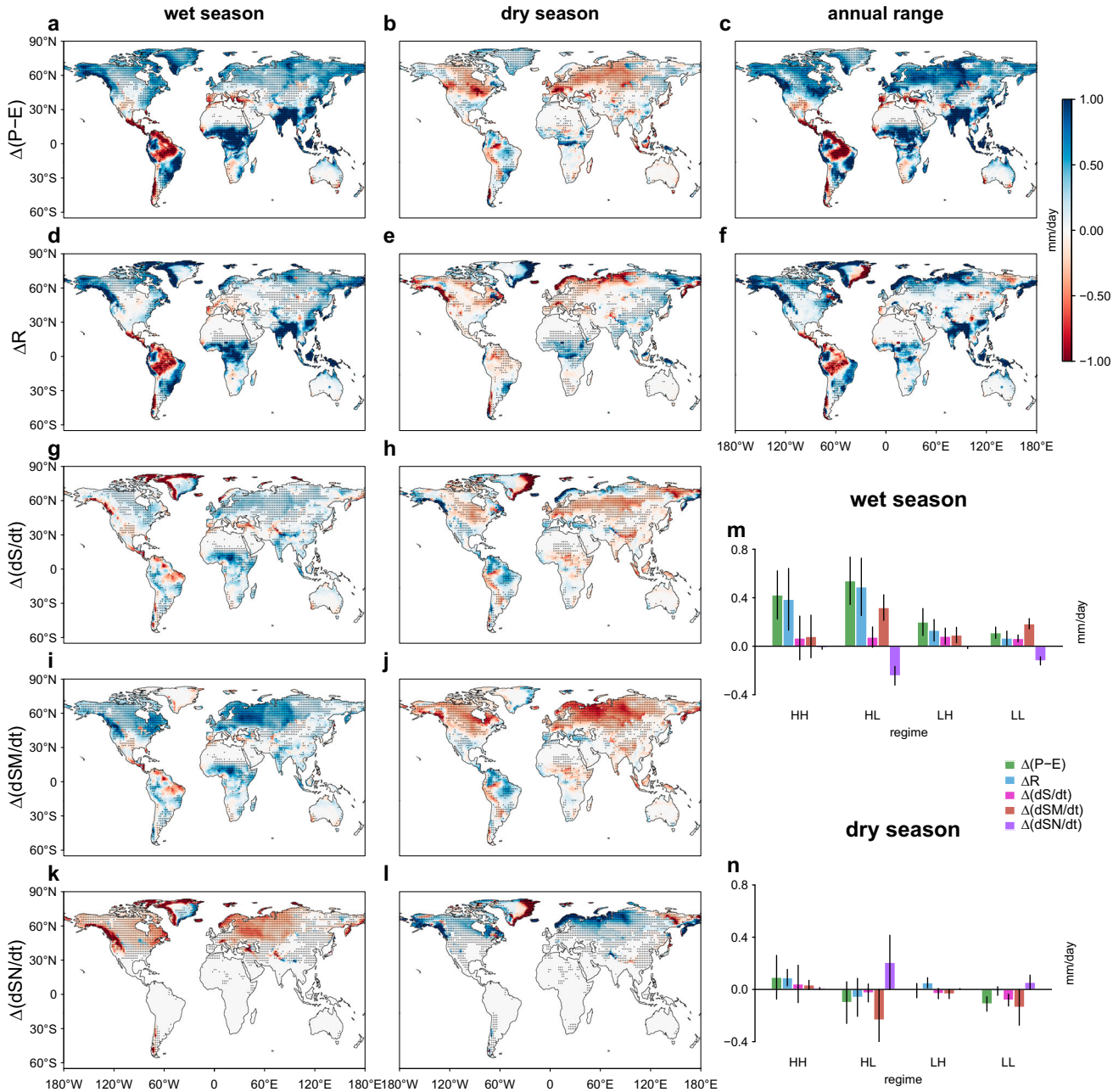

Fig. 3 | Multi-model mean seasonal changes in water availability between the historical and future periods. a–c Changes in water availability (Δ(P-E)) in the wet season (**a**) and the dry season (**b**), and their differences (i.e. the annual range of P-E, **c**) between the historical (1971–2000) and future (2071–2100, ssp5-8.5) periods. **d–l** The same as (**a**–**c**), but for runoff (R, **d**–**f**), changes in terrestrial water storage (d*S*/d*t*, **g**, **h**), soil moisture (d*SM*/d*t*, **i**, **j**), and snow amount (d*SN*/d*t*, **k**, **l**) over time during the wet and dry seasons. The dotted areas denote the sign of changes in the variables is consistent with the sign of multi-model means for more than 75% (at least 13) of the 17 models. **m**, **n** The area-weighted mean Δ(P-E), Δ*R*, Δ(d*S*/d*t*), Δ(d*SM*/d*t*) and Δ(d*SN*/d*t*) for the four regimes between the historical and future periods. The error bars show the standard deviations of the variables across the 17 models.

(HH and HL), future increases in precipitation are only partially offset by evaporation and contribute to greater increases in P-E (Figs. 2c and 4c, f). Changes in precipitation are predominantly offset by evaporation in the dry season, whereas increased precipitation significantly enhances P-E in the wet season (Figs. 3a–c and S9).

As precipitation increases are concentrated in wet months, while increases in evaporation are more evenly distributed (Fig. 4g–n), the divergent seasonal shifts in precipitation and evaporation affect P-E and hence runoff and terrestrial water storage in different ways. The considerably larger increases in wet-season precipitation relative to evaporation are responsible for the notable enhancements in wet-season P-E and runoff associated with the two wet regimes, particularly in central Africa and South and Southeast Asia (Figs. S9a, c and 3a, d). For the dry season, increased recharge of water storage during the wet season, coupled with heightened evaporative demand in a warming climate, accelerates evaporation that exceeds the increase in precipitation over many HL and LL regions (Fig. S9b, d, and f). This explains the faster declines in SM in future projections for the two low seasonality regimes (Fig. 3j, n). Overall, the concentrated increase in precipitation during the wet season, combined with a more evenly distributed increase in evaporation throughout the year, accounts for seasonal changes in runoff and water storage gain/loss. In particular, increases in precipitation play a predominant role in driving increases in runoff and

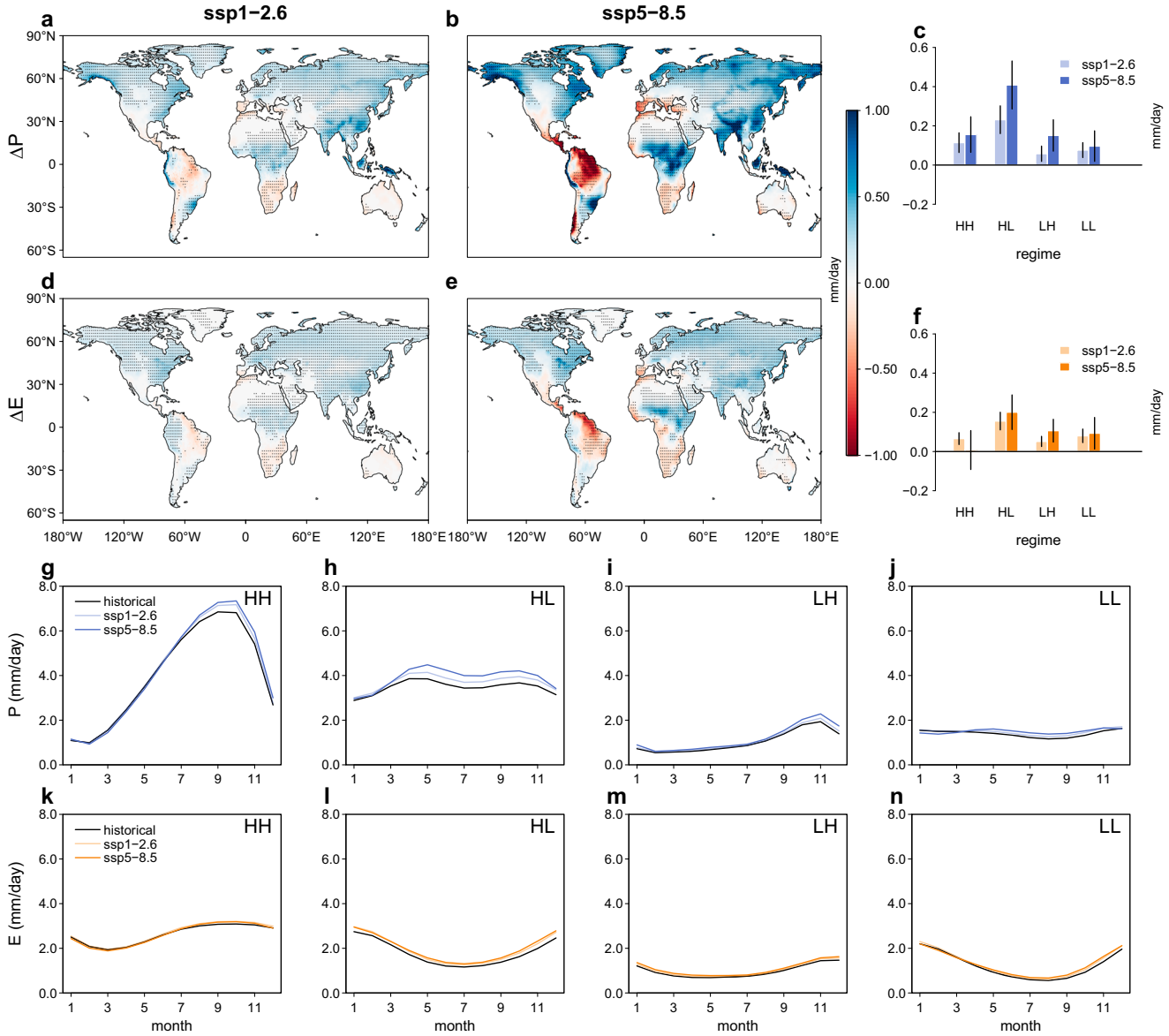

Fig. 4 | Multi-model mean changes in precipitation and evaporation between the historical and future periods. a–c Changes in precipitation (ΔP) between the historical (1971–2000) and future (2071–2100) periods under the ssp1-2.6 (**a**) and ssp5-8.5 (**b**) scenarios, and the area-weighted mean ΔP for the four regimes HH, HL, LH, and LL shown in Fig. 1. **d–f** The same as (**a–c**), but for changes in evaporation (ΔE). The dotted areas denote the sign of ΔP or ΔE is consistent with the sign of multi-model means for more than 75% (at least 13) of the 17 models. The error bars show the standard deviations of ΔP and ΔE across the 17 models. **g–n** Mean seasonal cycles of precipitation (**g–j**) and evaporation (**k–n**) for the four regimes during the historical and future (ssp1-2.6 and ssp5-8.5) periods. Month 1 along the *x*-axis is associated with the month with the lowest P-E during the historical period.

water storage gain in the wet season, while evaporation increases, along with reduced precipitation, are responsible for increased water storage losses in the dry season.

Discussion

Our study identifies the multifaceted climate change impacts on the terrestrial water cycle and water resources. By classifying the global terrestrial hydroclimate into four distinct regimes based on the multi-model ensemble of climatological mean P-E and precipitation seasonality, we find the spatial and temporal patterns of water availability are amplified over approximately half of the land areas. Such changes in P-E, due to coupled changes in the long-term mean and seasonal variability of precipitation and evaporation, significantly affect runoff and terrestrial water storage, but in different ways, for the four hydroclimate regimes. Increases in the mean P-E, particularly precipitation, and their amplified seasonality preferentially affect runoff for the HH regime, resulting in concentrated increases of 0.15–0.39 mm/d in runoff in the wet season. In contrast, the amplified seasonality of P-E results in more rapid SM increases by 0.08–0.19 mm/d in the wet season and particularly faster declines in SM by 0.07–0.14 mm/d during the dry season that may aggravate the water scarcity for the LL regime. For the HL regime, the enhanced seasonality of P-E contributes to the largest increases in runoff (0.19–0.49 mm/d) during the wet season and the strongest declines in SM (0.12–0.23 mm/d) during the dry season. These SM declines are pronounced in snow-covered regions, due to reduced seasonal cycles of snow accumulation and melt. The LH regime exhibits small increases in P-E, runoff, and terrestrial water storage in the wet season and more muted responses in the dry season, which may slightly alleviate the arid environment. As the climate change impacts vary greatly across different regimes, seasons, and hydroclimate variables, these findings underscore the necessity for continued assessment of multifaceted characteristics of forthcoming shifts in the terrestrial water cycle and water resources.

The comprehensive assessment of water cycle changes by considering both long-term averages and seasonality, as well as the hydroclimate regimes, sheds light on the most impactful aspects of climate change across different regions and has important implications for climate change adaptation. As P-E is projected to be more unevenly distributed over most land areas, water management adaptations, such as reservoirs and irrigation, are needed to address both water surplus and shortage issues, respectively, in wet and dry seasons[46,47]. Seasonal changes in precipitation, evaporation, runoff, soil moisture, and snow amount are also closely related to hydroclimate extremes, and may increase the likelihood of floods and droughts over different hydroclimate regimes. Indeed, an increase in flood events has been observed in the HH and HL regions, such as Europe[26] and eastern US[48], and they are projected to become more frequent and more severe in the future[49]. The frequency, intensity, and spatial extents of hydrological and agricultural droughts are also reported to increase in current and future climates[38,50–52], for example in the HL and LL regimes, likely due to reduced dry-season P-E, as well as the reduction of snow accumulation and snowmelt. The latter may disrupt the balance between water supply and demand in regions where societal and agricultural systems rely heavily on snowmelt runoff[44,45]. In addition, reduced snowmelt recharge, alongside enhanced evaporation under climate warming, accelerates SM declines during the dry season, heightening the risk of soil droughts and may trigger flash droughts[53] and compound droughts and heatwaves due to land-atmosphere feedbacks[54,55]. The observed and projected hydrological changes necessitate more efforts to mitigate floods and/or droughts and ensure continuous water supply throughout the year over different hydroclimate regimes.

Overall, our study disentangles the hydrological processes and unravels the multifaceted characteristics of hydrological changes under climate change. The projected changes in the terrestrial water cycle and water resources have profound implications for our society and ecosystems. The intensified seasonality in water availability presents significant challenges to local populations, making agricultural efforts and sustainable management of soil and water resources more difficult. Alterations in the mean and seasonal cycles in the key hydroclimate variables may also signify substantial and varied shifts in vegetation activities, ecosystem functioning, and terrestrial carbon cycle[56,57]. These coupled changes in the human-nature system offer valuable insights into societal and ecological vulnerability to climate change, facilitating the development of mitigation and adaptation strategies. It is worth noting that the projected hydrological changes have not considered the impact of direct human activities, such as land use and land cover changes and water resources management, which may further accentuate or alleviate the climate change impacts[58,59]. It is crucial to maintain ongoing monitoring and forecasting of the complex hydrological changes by integrating multiple dimensions of human impacts on the global and regional water resources and developing policies and strategies to reduce vulnerability to water-related disasters.

Methods

CMIP6 model simulations

We used monthly outputs of precipitation ("pr), evaporation ("evspsbl"), runoff ("mrro"), total soil moisture content ("mrso"), and surface snow amount ("snw") from 17 climate models in CMIP6 (Table S1). These models were selected because they have archived the required variables in the historical (1850—2014) and future (2015–2100) simulations under two emission scenarios: the low forcing sustainability pathway (ssp1-2.6) and the high-end forcing pathway (ssp5-8.5), in which the radiative forcing reaches 2.6 W/m^2 and 8.5 W/m^2, respectively, by 2100. Moreover, these models have accurately simulated the climatological water balance, i.e. precipitation equals the sum of runoff and evaporation at the 30-year scale, over land grid cells and well represented the water balance in dry and wet seasons by considering seasonal changes in terrestrial water storage. As CMIP6 models do not include groundwater modelling and glacier mass changes, terrestrial water storage was calculated as the sum of total soil moisture content and surface snow amount at the monthly scale, provided that these components are simulated independently[60]. Several models, in which the simulated soil moisture and snow amount are not fully independent, i.e. sharing core elements or treated as extensions from each other, were not used to minimize systematic errors in terrestrial water storage and surface water balance. Finally, the 17 models that have met the climatological and seasonal water balance requirements were selected for data analyses. We used one ensemble member from each model (see Table S1), as simulations from different members of a given model are quite similar, differing only in initial conditions while maintaining identical anthropogenic climate forcings. The model outputs were bilinearly resampled to a common spatial resolution of $1° \times 1°$ to obtain the multi-model ensemble mean.

ERA5 reanalysis and observation-based datasets

To assess the global distribution of hydroclimate regimes, we used evaporation and precipitation data from ERA5 global reanalysis[34]. As the ERA5 reanalysis is constrained with in situ and satellite remote-sensing observations, it provides a reliable representation of hydroclimate characteristics worldwide. For our analysis, we used monthly outputs of evaporation and precipitation at the spatial resolution of $1° \times 1°$ for the period 1971–2000 to identify the historical hydroclimate regimes (see "Definition of hydroclimate regimes" below). Additionally, we used observation-based datasets of GPCC precipitation[35] and GLEAM evaporation[36] to evaluate model simulations in the historical period (1971–2000).

Definition of hydroclimate regimes

To characterize hydroclimate regimes over different regions, we consider both the climatological mean water availability (P-E) and its seasonality. While precipitation is commonly used to represent the water constraint for a given region[15,61], the spatial and temporal patterns of water availability, along with regional hydroclimate characteristics, are influenced by both precipitation and evaporation. The climatological mean P-E measures the amount of water resources that are theoretically available for humans and ecosystems for a given region, accounting for water input via precipitation and losses through evaporation. Seasonality characterizes how water resources are distributed between different seasons and defines regional water supply patterns. It also influences the occurrence and characteristics of hydroclimate extremes, such as droughts and floods, and has crucial implications for the sustainable management of water resources. As the seasonal cycle of P-E is largely driven by that of precipitation (Fig. 1), we quantified the hydroclimate seasonality based on the relative entropy (RE) of precipitation, which has been widely adopted to evaluate the precipitation seasonality from a non-parametric standpoint[19,32,62].

The RE of precipitation for the historical period (1971–2000) was estimated for each grid cell in each model as follows:

1. the historical mean precipitation was obtained for each of the 12 months, i.e. P_m, $m \in [1, 12]$;
2. the probability distribution of mean monthly precipitation (p_m) was computed as

$$p_m = \frac{P_m}{\sum_{m=1}^{12} P_m}, p_m \in [0, 1] \quad (1)$$

3. the RE of mean precipitation was estimated to measure whether the precipitation distribution is similar to a uniform distribution with the same probability of 1/12 for each month, i.e. $q_m = \frac{1}{12}$, for all m,

$$\mathrm{RE} = \sum_{m=1}^{12} p_m \log_2\left(\frac{p_m}{q_m}\right), \mathrm{RE} \in \left[0, \log_2 12\right] \quad (2)$$

where $\mathrm{RE} = 0$ when precipitation is uniformly distributed, i.e. $p_m = q_m = \frac{1}{12}$. RE increases as precipitation becomes more seasonally variable and reaches its maximum value of $\log_2 12$ (= 3.585) when all annual precipitation is concentrated in one month. The larger the RE value, the higher the variability in monthly precipitation, and a higher hydroclimate seasonality.

We utilized a multi-model ensemble approach to classify global terrestrial hydroclimate into four distinct regimes, ensuring that this classification effectively captures historical hydroclimate characteristics and is broadly representative across different models. Using multi-model mean P-E and RE for the historical period, we defined four hydroclimate regimes based on the median (i.e. 50th percentile) thresholds of P-E and RE across land grid cells: high/low P-E and high/low seasonality (Fig. 1). This classification of hydroclimate regimes combines the mean and seasonality to better capture regional hydroclimate characteristics and allows us to evaluate future changes in the climatological means and seasonal cycles of hydroclimate variables for different regimes/regions. Considering model differences in hydroclimate simulations, we used only four regimes so that different models could achieve a high level of consistency in terms of the classification results (Fig. S2). The global distribution of the four regimes based on the multi-model ensemble is consistent with the distribution derived from the ERA5 reanalysis (Fig. S1a). Additionally, the multi-model mean seasonal cycles of precipitation, evaporation, and P-E, along with their historical changes, align closely with those from ERA5 (Fig. S1c–n). This indicates that the multi-model ensemble could well capture the global hydroclimate characteristics. We have also tried another classification scheme using quantile-based thresholds (e.g. the 30th and 70th percentiles), resulting in a classification of nine regimes in total. However, the results varied greatly across different models, indicating that the classification outcomes might not effectively capture hydroclimate characteristics consistently across different models.

To examine whether the historical hydroclimate regimes are representative of future hydroclimate characteristics, we also identified four hydroclimate regimes based on future simulations (2071–2100, ssp5-8.5). The spatial distribution and land area of the four regimes between the historical and future periods are similar (Fig. 1 and S3), indicating that the hydroclimate regimes are relatively consistent despite changes in P-E and RE driven by anthropogenic climate change. Overall, the multi-model ensemble effectively captures historical hydroclimate characteristics across different models and time periods, allowing a robust assessment of changes in water availability in a warming climate.

Changes in surface water balance

Surface water balance dictates that precipitation (P) minus evaporation (E), i.e. the surface water availability, equals the sum of runoff (R) and changes in terrestrial water storage with time ($\mathrm{d}S/\mathrm{d}t$):

$$P - E = R + \mathrm{d}S/\mathrm{d}t \tag{3}$$

where $\mathrm{d}S/\mathrm{d}t$ represents the sum of changes in soil moisture ($\mathrm{d}SM/\mathrm{d}t$) and snow amount ($\mathrm{d}SN/\mathrm{d}t$) over time. At the monthly scale, P-E can be directly calculated using model outputs of precipitation and evaporation. Changes in terrestrial water storage, $\mathrm{d}S/\mathrm{d}t$, should be calculated as the difference in water storage at the beginning and the end of each month. However, as daily water storage was not available in many climate models, $\mathrm{d}S/\mathrm{d}t$ for month i, i.e. $\left(\mathrm{d}S/\mathrm{d}t\right)_i$, was usually evaluated using water storage changes between two adjacent months calculated from the forward ($S_{i+1} - S_i$) or backward ($S_i - S_{i-1}$) difference method[63], or the combination of the two methods (Eq. (4)).

$$\left(\mathrm{d}S/\mathrm{d}t\right)_i = \frac{S_{i+1} - S_{i-1}}{2} \tag{4}$$

While the seasonal cycles of $\mathrm{d}S/\mathrm{d}t$ calculated from the three methods are quite similar, the combination method, i.e. Eq. (4), could better ensure surface water balance (Eq. (3)) for most land areas and was used to obtain monthly $\mathrm{d}S/\mathrm{d}t$ and its components ($\mathrm{d}SM/\mathrm{d}t$ and $\mathrm{d}SN/\mathrm{d}t$) in this study.

To assess future hydrological changes, we compared the climatological mean and seasonal variations in the hydroclimate variables (i.e. P, E, P-E, R, $\mathrm{d}S/\mathrm{d}t$, $\mathrm{d}SM/\mathrm{d}t$, $\mathrm{d}SN/\mathrm{d}t$) between the historical (1971–2000) and future (2071–2100) periods. To characterize the seasonal cycle, the month with the lowest mean P-E during the historical period is taken as the starting month of a year for each grid cell in each model. Following the previous analysis[13], the dry and wet seasons are defined as three consecutive months with the lowest and highest mean P-E during the historical period. While the driest and wettest months/seasons may change in future simulations, we used the same definitions of dry and wet seasons for both historical and future periods, which enable us to better compare future changes in the seasonal cycles of surface water balance under different forcing scenarios (i.e. ssp1-2.6 and ssp5-8.5).

We examined the robustness of long-term and seasonal hydrological changes based on the multi-model agreement. Taking the change in P-E (Δ(P-E)) as an example, Δ(P-E) is deemed to be statistically significant (p-value < 0.05) if the sign of change is the same as that of the multi-model mean Δ(P-E) in at least 13 of the 17 models[13]. This is because the likelihood of Δ(P-E) to be either positive or negative is 50%, assuming there is no consistent change in P-E between the historical and future periods. To test this null hypothesis, we calculated the probability that at least 13 of the 17 models would have the same sign as the multi-model mean using the binomial distribution[13].

$$P(n \geq 13) = \sum_{n=13}^{17} \frac{17!}{n!(17-n)!} 0.5^n \times 0.5^{(17-n)} < 0.05 \tag{5}$$

Equation (5) suggests that the null hypothesis of no change could be rejected and the change in P-E is significant at the 95% confidence level. Similarly, we examined whether changes in other hydroclimate variables are significant based on agreement in sign for at least 13 (>75%) of the 17 CMIP6 models.

Data availability

All data used in this study are available online. The CMIP6 model simulations are publicly available from https://esgf-node.llnl.gov/search/cmip6/. The ERA5 reanalysis is available from https://cds.climate.copernicus.eu/datasets/reanalysis-era5-single-levels-monthly-means?tab=overview. The GLEAM evaporation is available from https://www.gleam.eu/. The GPCC precipitation is available from https://opendata.dwd.de/climate_environment/GPCC/html/download_gate.html.

Code availability

The R code used for data analyses is available upon request.

Received: 14 September 2024; Accepted: 10 January 2025;
Published online: 24 January 2025

References

1. Greve, P. et al. Global assessment of trends in wetting and drying over land. *Nat. Geosci.* **7**, 716–721 (2014).
2. Rodell, M. et al. Emerging trends in global freshwater availability. *Nature* **557**, 651–659 (2018).
3. Zaitchik, B. F., Rodell, M., Biasutti, M. & Seneviratne, S. I. Wetting and drying trends under climate change. *Nat. Water* **1**, 502–513 (2023).
4. Allan, R. P. et al. Advances in understanding large-scale responses of the water cycle to climate change. *Ann. N. Y. Acad. Sci.* **1472**, 49–75 (2020).
5. Huggins, X. et al. Hotspots for social and ecological impacts from freshwater stress and storage loss. *Nat. Commun.* **13**, 439 (2022).
6. Huntington, T. G. Evidence for intensification of the global water cycle: Review and synthesis. *J. Hydrol.* **319**, 83–95 (2006).
7. Chou, C. et al. Increase in the range between wet and dry season precipitation. *Nat. Geosci.* **6**, 263–267 (2013).
8. Byrne, M. P. & O'Gorman, P. A. The response of precipitation minus evapotranspiration to climate warming: why the "Wet-Get-Wetter, Dry-Get-Drier" scaling does not hold over land. *J. Clim.* **28**, 8078–8092 (2015).
9. Allan, R. P. Amplified seasonal range in precipitation minus evaporation. *Environ. Res. Lett.* **18**, 094004 (2023).

10. Ficklin, D. L., Null, S. E., Abatzoglou, J. T., Novick, K. A. & Myers, D. T. Hydrological intensification will increase the complexity of water resource management. *Earth's. Future* **10**, e2021EF002487 (2022).
11. Chou, C., Neelin, J. D., Chen, C.-A. & Tu, J.-Y. Evaluating the "Rich-Get-Richer" mechanism in tropical precipitation change under global warming. *J. Clim.* **22**, 1982–2005 (2009).
12. Zhou, S. et al. Soil moisture–atmosphere feedbacks mitigate declining water availability in drylands. *Nat. Clim. Chang.* **11**, 38–44 (2021).
13. Zhou, S. et al. Diminishing seasonality of subtropical water availability in a warmer world dominated by soil moisture–atmosphere feedbacks. *Nat. Commun.* **13**, 5756 (2022).
14. Duan, S. Q., Findell, K. L. & Fueglistaler, S. A. Coherent mechanistic patterns of tropical land hydroclimate changes. *Geophys. Res. Lett.* **50**, e2022GL102285 (2023).
15. Konapala, G., Mishra, A. K., Wada, Y. & Mann, M. E. Climate change will affect global water availability through compounding changes in seasonal precipitation and evaporation. *Nat. Commun.* **11**, 3044 (2020).
16. Koutsoyiannis, D. Revisiting the global hydrological cycle: Is it intensifying? *Hydrol. Earth Syst. Sci.* **24**, 3899–3932 (2020).
17. Kumar, S., Allan, R. P., Zwiers, F., Lawrence, D. M. & Dirmeyer, P. A. Revisiting trends in wetness and dryness in the presence of internal climate variability and water limitations over land. *Geophys. Res. Lett*. **42**, 10,867–0,875 (2015).
18. Lin, S. et al. The seasonal variability of future evapotranspiration over China during the 21st century. *Sci. Total Environ.* **926**, 171816 (2024).
19. Pascale, S., Lucarini, V., Feng, X., Porporato, A. & Hasson, S. U. Analysis of rainfall seasonality from observations and climate models. *Clim. Dyn.* **44**, 3281–3301 (2015).
20. Zhou, S. et al. Large divergence in tropical hydrological projections caused by model spread in vegetation responses to elevated CO_2. *Earth's Future* https://doi.org/10.1029/2021EF002457 (2022).
21. Kumar, S., Lawrence, D. M., Dirmeyer, P. A. & Sheffield, J. Less reliable water availability in the 21st century climate projections: KUMAR ET AL. *Earth's. Future* **2**, 152–160 (2014).
22. Kreibich, H. et al. The challenge of unprecedented floods and droughts in risk management. *Nature* **608**, 80–86 (2022).
23. Tabari, H., Hosseinzadehtalaei, P., Thiery, W. & Willems, P. Amplified drought and flood risk under future socioeconomic and climatic change. *Earth's Future* https://doi.org/10.1029/2021EF002295 (2021).
24. Lan, H. et al. Climate change drives flooding risk increases in the Yellow River Basin. *Geogr. Sustainability* **5**, 193–199 (2024).
25. Zhou, S., Yu, B., Lintner, B. R., Findell, K. L. & Zhang, Y. Projected increase in global runoff dominated by land surface changes. *Nat. Clim. Chang.* **13**, 442–449 (2023).
26. Blöschl, G. et al. Current European flood-rich period exceptional compared with past 500 years. *Nature* **583**, 560–566 (2020).
27. Zhang, S. et al. Reconciling disagreement on global river flood changes in a warming climate. *Nat. Clim. Chang.* **12**, 1160–1167 (2022).
28. Ault, T. R. On the essentials of drought in a changing climate. *Science* **368**, 256–260 (2020).
29. Hoffmann, D., Gallant, A. J. E. & Hobbins, M. Flash drought in CMIP5 models. *J. Hydrometeorol*. https://doi.org/10.1175/JHM-D-20-0262.1 (2021).
30. Yuan, X. et al. A global transition to flash droughts under climate change. *Science* **380**, 187–191 (2023).
31. Eyring, V. et al. Overview of the coupled model intercomparison project phase 6 (CMIP6) experimental design and organization. *Geosci. Model Dev.* **9**, 1937–1958 (2016).
32. Feng, X., Porporato, A. & Rodriguez-Iturbe, I. Changes in rainfall seasonality in the tropics. *Nat. Clim. Change* **3**, 811–815 (2013).
33. Wainwright, C. M., Allan, R. P. & Black, E. Consistent trends in dry spell length in recent observations and future projections. *Geophys. Res. Lett.* **49**, e2021GL097231 (2022).
34. Hersbach, H. et al. The ERA5 global reanalysis. *Q. J. R. Meteorol. Soc.* **146**, 1999–2049 (2020).
35. Becker, A. et al. A description of the global land-surface precipitation data products of the Global Precipitation Climatology Centre with sample applications including centennial (trend) analysis from 1901–present. *Earth Syst. Sci. Data* **5**, 71–99 (2013).
36. Miralles, D. G. et al. GLEAM4: global land evaporation dataset at 0.1° resolution from 1980 to near present. *Springer Science and Business Media LLC* https://doi.org/10.21203/rs.3.rs-5488631/v1 (2024).
37. Singh, D., Tsiang, M., Rajaratnam, B. & Diffenbaugh, N. S. Observed changes in extreme wet and dry spells during the South Asian summer monsoon season. *Nat. Clim. Change* **4**, 456–461 (2014).
38. Cook, B. I. et al. Twenty-first century drought projections in the CMIP6 forcing scenarios. *Earth's. Future* **8**, e2019EF001461 (2020).
39. Trancoso, R. et al. Significantly wetter or drier future conditions for one to two thirds of the world's population. *Nat. Commun.* **15**, 483 (2024).
40. Bintanja, R. & Andry, O. Towards a rain-dominated Arctic. *Nat. Clim. Change* **7**, 263–267 (2017).
41. O'Gorman, P. A. Contrasting responses of mean and extreme snowfall to climate change. *Nature* **512**, 416–418 (2014).
42. Barnett, T. P., Adam, J. C. & Lettenmaier, D. P. Potential impacts of a warming climate on water availability in snow-dominated regions. *Nature* **438**, 303–309 (2005).
43. Barnhart, T. B. et al. Snowmelt rate dictates streamflow: snowmelt rate dictates streamflow. *Geophys. Res. Lett.* **43**, 8006–8016 (2016).
44. Qi, W., Feng, L., Liu, J. & Yang, H. Snow as an important natural reservoir for runoff and soil moisture in northeast China. *J. Geophys. Res.: Atmospheres* **125**, e2020JD033086 (2020).
45. Qin, Y. et al. Agricultural risks from changing snowmelt. *Nat. Clim. Chang.* **10**, 459–465 (2020).
46. Oki, T. & Kanae, S. Global hydrological cycles and world water resources. *Science* **313**, 1068–1072 (2006).
47. Yang, D., Yang, Y. & Xia, J. Hydrological cycle and water resources in a changing world: a review. *Geogr. Sustainability* **2**, 115–122 (2021).
48. Wing, O. E. J. et al. Inequitable patterns of US flood risk in the Anthropocene. *Nat. Clim. Chang.* **12**, 156–162 (2022).
49. Hirabayashi, Y., Tanoue, M., Sasaki, O., Zhou, X. & Yamazaki, D. Global exposure to flooding from the new CMIP6 climate model projections. *Sci. Rep.* **11**, 3740 (2021).
50. Dai, A. Increasing drought under global warming in observations and models. *Nat. Clim. Change* **3**, 52–58 (2013).
51. Rodell, M. et al. An abrupt decline in global terrestrial water storage and its relationship with sea level change. *Surv. Geophys* **45**, 1875–1902 (2024).
52. Song, J. et al. Serious underestimation of reduced carbon uptake due to vegetation compound droughts. *npj Clim. Atmos. Sci.* **7**, 23 (2024).
53. Potopová, V., Boroneanț, C., Možný, M. & Soukup, J. Driving role of snow cover on soil moisture and drought development during the growing season in the Czech Republic. *Int. J. Climatol.* **36**, 3741–3758 (2016).
54. Gloege, L. et al. Land-atmosphere cascade fueled the 2020 Siberian heatwave. *AGU Advances* https://doi.org/10.1029/2021AV000619 (2022).
55. Zhou, S. et al. Land–atmosphere feedbacks exacerbate concurrent soil drought and atmospheric aridity. *PNAS* **116**, 18848–18853 (2019).
56. Gentine, P. et al. Coupling between the terrestrial carbon and water cycles—a review. *Environ. Res. Lett.* **14**, 083003 (2019).
57. Zhang, Y. et al. Increasing sensitivity of dryland vegetation greenness to precipitation due to rising atmospheric CO_2. *Nat. Commun.* **13**, 4875 (2022).

58. Sterling, S. M., Ducharne, A. & Polcher, J. The impact of global land-cover change on the terrestrial water cycle. *Nat. Clim. Change* **3**, 385–390 (2013).
59. Ma, S., Zhou, S., Yu, B. & Song, J. Deforestation-induced runoff changes dominated by forest-climate feedbacks. *Sci. Adv.* **10**, eadp3964 (2024).
60. Jensen, L., Eicker, A., Dobslaw, H. & Pail, R. Emerging changes in terrestrial water storage variability as a target for future satellite gravity missions. *Remote Sens.* **12**, 3898 (2020).
61. Zhou, S. et al. A new method to partition climate and catchment effect on the mean annual runoff based on the Budyko complementary relationship. *Water Resour. Res.* **52**, 7163–7177 (2016).
62. Pascale, S., Lucarini, V., Feng, X., Porporato, A. & Ul Hasson, S. Projected changes of rainfall seasonality and dry spells in a high greenhouse gas emissions scenario. *Clim. Dyn.* **46**, 1331–1350 (2016).
63. Zhao, M., A, G., Liu, Y. & Konings, A. G. Evapotranspiration frequently increases during droughts. *Nat. Clim. Chang.* **12**, 1024–1030 (2022).

Acknowledgements

We acknowledge the World Climate Research Programme's Working Group on Coupled Modelling, which is responsible for CMIP, and we thank the climate modelling groups for producing and making available their model output. For CMIP the U.S. Department of Energy's Programme for Climate Model Diagnosis and Intercomparison provides coordinating support and led development of software infrastructure in partnership with the Global Organization for Earth System Science Portals. This work was supported by the National Key Research and Development Programme of China (2022YFF0801303), the NSFC Excellent Young Scientists Fund (Overseas), and the Fundamental Research Funds for the Central Universities.

Author contributions

S.Z. conceived and designed the study. B.G. processed model simulations. B.Y., K.L.F., and B.R.L. contributed to data analysis and interpretation. S.Z. and B.G. wrote the manuscript. All authors edited the manuscript.

Competing interests

The authors declare no competing interests.

Additional information

Supplementary information The online version contains supplementary material available at https://doi.org/10.1038/s41612-025-00913-4.

Correspondence and requests for materials should be addressed to Sha Zhou.